

Article

Adsorption Process of Methyl Orange Dye onto Zinc Hydroxide Nitrate: Kinetic and Thermodynamic Studies

Daiane Amaral de Ramos Nogueira, Tânia Marina Palhano Zanela, Monielly Viomar Machado, Carlos Alberto Policiano Almeida and Rafael Marangoni * 

Departamento de Química (DEQ), Universidade Estadual do Centro-Oeste (UNICENTRO), Guarapuava 85040-167, PR, Brazil; dnogueira.unicentro@outlook.com (D.A.d.R.N.); palhano.tania@hotmail.com (T.M.P.Z.); monnvm@hotmail.com (M.V.M.); policiano@unicentro.br (C.A.P.A.)

* Correspondence: rmarangoni@unicentro.br

Abstract: Zinc hydroxide nitrate (ZHN) was used as an anionic adsorbent for the removal of methyl orange (MO) dye from aqueous solutions. ZHN was characterized via X-ray diffraction (XRD) and infrared spectroscopy (FTIR) techniques. Investigations were carried out to see how the adsorption of MO was affected by factors such as initial MO concentration, contact time and temperature. Adsorption isotherms were analyzed using the Langmuir and Freundlich equations, with the first one being the better result for the equilibrium data. Adsorption kinetics was studied through applying pseudo-first and pseudo-second-order kinetic models, and the experimental data were better fitted to the pseudo-second-order model. The activation energy was determined using the Arrhenius equation to be $105.45 \text{ kJ mol}^{-1}$, revealing the chemical nature of the adsorption process. The thermodynamic parameters were also determined, showing the adsorption of MO onto ZHN to be a non-spontaneous and exothermic process. The experimental results showed ZHN as a potential adsorbent with adsorption capacity for removing anionic dyes from water medium.

Keywords: adsorption; methyl orange dye; layered hydroxide salts; zinc hydroxide nitrate



Citation: Nogueira, D.A.d.R.; Zanela, T.M.P.; Machado, M.V.; Almeida, C.A.P.; Marangoni, R. Adsorption Process of Methyl Orange Dye onto Zinc Hydroxide Nitrate: Kinetic and Thermodynamic Studies. *Colorants* **2023**, *2*, 565–577. <https://doi.org/10.3390/colorants2030028>

Academic Editor: Anthony Harriman

Received: 30 July 2023

Revised: 26 August 2023

Accepted: 31 August 2023

Published: 6 September 2023



Copyright: © 2023 by the authors. Licensee MDPI, Basel, Switzerland. This article is an open access article distributed under the terms and conditions of the Creative Commons Attribution (CC BY) license (<https://creativecommons.org/licenses/by/4.0/>).

1. Introduction

The disposal of dyes, organic pollutants and inorganic heavy metal ions into the environment from industrial waste effluents without any previous treatment has caused severe environmental problems [1,2].

Effluents contaminated by dyes, if not correctly treated before disposal into rivers, are easily noticeable, even in low dye concentrations. Besides visual pollution, the presence of dyes in water also causes damage in the biological cycle, modifying the ecosystem and mainly affecting the photosynthesis process [3–5]. As long as industrial growth and development tend to keep pace with population consumption, this problem becomes even more worrying.

At present, there are many techniques of wastewater treatment, but none of them are completely satisfactory. Among them, adsorption has been an efficient technique for removing dyes from effluents due to its low cost, flexibility, simplicity and easy operation [6]. The adsorption process is defined as the accumulation of a substance (adsorbate) in the interface between the solid surface (adsorbent) and the adjacent solution.

Several adsorbents have been used in adsorption processes, including activated carbon, agricultural wastes, nanomaterials and modified compounds. Layered hydroxide salts (LHSs) are compounds with optimal characteristics related to porosity, large surface area, easy production and low cost [7] to be used as adsorbents in the adsorption process. Another important feature is the possibility of reusing or functionalizing these materials through ion exchange [8].

LHSs are classified as layered compounds with atoms strongly linked by covalent bonds through weak forces of Van der Waals, forming two-dimensional structures [9,10].

LHSs' layered structure is similar to that of brucite, containing a coordinated interaction between the central metal with hydroxyl groups forming regular octahedron sites with the general formula $M^{2+}(\text{OH})_{x-y}\text{B}_y \cdot n\text{H}_2\text{O}$ [11,12]. Zinc hydroxide nitrate (ZHN) is an example of a layered structure of the general formula $\text{Zn}_5(\text{OH})_8(\text{NO}_3)_2 \cdot 2\text{H}_2\text{O}$, where the intercalated anion is not coordinated directly with the metal.

LHS compounds have been used as precursors of metal oxides with topotactic growth [7], topotactic reaction of divalent cations [13], epitaxial film [14], catalysts for esterification of fatty acids [9], anionic exchangers with properties of selective retention of anions [15], magnetic property materials [16], among others, but there are few studies describing LHS as an adsorbent [17,18].

ZHN compounds are widely studied due to their functional groups that allow the intercalation of chemical species (anions, cations, atoms and macromolecules) between the layers, giving them functional features, such as the transport or storage of energy [19,20].

Methyl orange (MO) is a sulfonated azo dye utilized not only in textile dyeing but also in biomedical applications as a pH indicator. MO and other azo dye metabolites are potentially carcinogenic, teratogenic, mutagenic and very recalcitrant in nature. MO has a complex structure and is difficult to biodegrade when subjected to heat, light, and chemical compounds. As a result, before being released into the environment, MO-containing effluent should be decolorized and detoxified. MO is a common type of carcinogenic anionic azo dye and can be used as a model for studies with azo dyes. Thus, research on MO adsorption is practical and helpful in comparing results from diverse investigations [21,22].

The main purpose of this study was to assess the adsorption potential of ZHN to remove MO from aqueous solutions. Therefore, this study investigated the effects of adsorbent dosage, contact time and thermodynamic and kinetic parameters.

2. Materials and Methods

2.1. Chemicals and Reagents

Zinc nitrate hexahydrate ($\text{Zn}(\text{NO}_3)_2 \cdot 6\text{H}_2\text{O}$; M.W. 297.49 g mol⁻¹, Synth, 96%) and sodium hydroxide (NaOH; M.W. 40.00 g mol⁻¹, Neon, 97%) were used. MO, used as the adsorbate, is an anionic dye (chemical formula, $\text{C}_{14}\text{H}_{14}\text{N}_3\text{NaO}_3\text{S}$; M.W. 327.33 g mol⁻¹; C.I.13025), with a maximum absorbance peak at $\lambda_{\text{max}} = 465$ nm and a chemical structure that is shown in Figure 1.

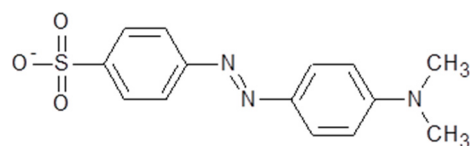


Figure 1. The chemical structure of MO.

It was obtained from Vetec and used without further purification. A stock solution of MO was prepared by dissolving an accurately weighed amount of MO in distilled water to achieve a concentration of 2000 mg L⁻¹ and was stored in an appropriate flask for further dilution to the required concentrations. All chemicals used in this study were of analytical laboratory grade.

2.2. Synthesis of Zinc Hydroxide Nitrate (ZHN)

The synthesis of ZHN, $\text{Zn}_5(\text{OH})_8(\text{NO}_3)_2 \cdot 2\text{H}_2\text{O}$, was carried out using the chemical co-precipitation method at room temperature (25 °C), according to the studies of Cordeiro et al. as follows [11]. Zinc nitrate hexahydrate (23.0 g) was dissolved in distilled water (80 mL, 0.96 mol L⁻¹) under magnetic stirring, and a sodium hydroxide solution (1 mol L⁻¹) was dripped utilizing a peristaltic pump at a speed of 3 rpm. The mixture remained under stirring for 4 h. A precipitate has been formed, washed five times with distilled water to remove the excess of free ions present in the solution, and oven-dried at 70 °C. The product,

at a yield of 80%, was characterized via X-ray diffraction (XRD) and Fourier transform infrared (FTIR) spectroscopy.

2.3. Adsorption Experiments

Batch uptake studies were carried out by stirring (450 rpm) 0.1 g of ZHN with 50 mL of unbuffered MO solutions of several different initial concentrations (100 mg L⁻¹ to 1000 mg L⁻¹) prepared from the stock solution of 2000 mg L⁻¹, in 80 mL glass cells. The adsorption study was conducted for three hours at different temperatures (25, 45 and 55 °C) in a thermostated system with an outer circulating water bath. Aliquots of the MO solutions were collected at regular time intervals, diluted, and centrifuged for 10 min at 2000 rpm. The absorbance measurements of the supernatant solutions were analyzed using a UV-vis spectrophotometer using a 1 cm path-length cell at $\lambda_{\max} = 465$ nm (maximum absorbance). The amount of MO adsorbed by the ZHN during the adsorption process in each time interval t , q_t (mg g⁻¹), was calculated using the mass balance equation, given as Equation (1):

$$q_t = (C_0 - C_t) \frac{V}{m} \quad (1)$$

where, C_0 and C_t are, respectively, the initial and liquid-phase concentrations of the MO solution (mg L⁻¹) at any time t ; V is the volume of the MO solution (ca. 0.05 L); and m is the mass of the ZHN used (ca. 0.10 g).

2.4. Characterizations

X-ray diffraction (XRD) measurements were performed on a BRUKER diffractometer, model D2 PHASER, equipped with Cu K α radiation ($\lambda = 1.5418$ Å) operating at 30 kV and 10 mA. Data were collected in a step scan mode between 5.0° and 20° (2 θ) with a step size of 0.2°/s.

Infrared (FTIR) measurements were collected in a Thermo Electron Corporation Nicolet IR 200 spectrometer using dried KBr tablets containing 1 wt% of the samples. The analyses of all samples were performed in the 4000 to 400 cm⁻¹ region with a resolution of 4 cm⁻¹, through accumulating 64 scans.

UV-Vis spectrophotometer of FEMTO 800XI with a 1 cm path-length cell was used to measure the absorbance of the supernatant solutions at 465 nm (maximum absorbance of methyl orange).

3. Results and Discussion

3.1. ZHN and ZHN-MO Characterizations

Figure 2 shows X-ray diffractograms of the ZHN samples before (a) and after (b and c) MO adsorption at different initial adsorbate concentrations at 25 °C.

X-ray diffractogram of ZHN (Figure 2a) shows diffraction peaks at 9.01° 2 θ (001) and 18.02° 2 θ (002) (tagged with • in Figure 2). The peak at 9.01° corresponds to the crystalline structure with a basal distance of 9.64 Å. The basal distance was calculated according to the highest-order basal peak of the ZHN diffractogram, and the value is consistent with the ones found in the literature [23].

The X-ray diffractograms of the ZHN-MO samples at two different concentrations in Figure 2b,c show a lower intensity of the peak at 9.01° 2 θ angle when compared to the ZHN peak, where the basal distance increased from 9.64 Å to 9.86 Å. The peaks at 7.33° (002), 11.06° (003) and 14.82° (004) (tagged with * in Figure 2b,c) correspond to a new phase present on ZHN-MO. The new phase observed is due to the intercalation of dye molecules in the interlayer space with a basal distance of around 23.9 Å (peak (001)) to ZHN-MO.

The FTIR spectra of MO (a), ZHN-MO (b) and ZHN (c) are shown in Figure 3. The spectrum of ZHN (c) has prominent broad absorption at around 3570 cm⁻¹, attributed to the O-H stretching modes, and 3483 cm⁻¹, related to the stretching vibrations, while 1630 cm⁻¹ is related to the O-H angular deformation of water molecules. The band related to O-H stretching has less intensity in (b) than in (c). In the (b) spectrum, the band related

to the angular deformation vibrations of the hydroxyls disappeared, suggesting an ionic exchange of the nitrate ions bounded to these hydroxyls for the dye molecules [24,25].

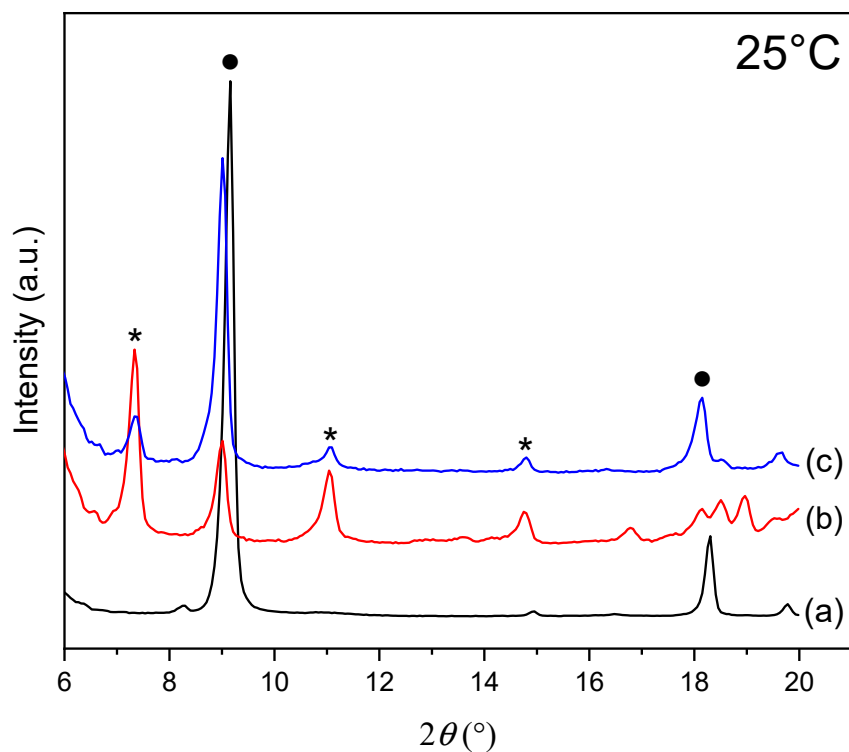


Figure 2. X-ray diffraction patterns of the samples at 25 °C: (a) for the ZHN sample; (b) for the ZHN-MO sample for the initial concentration of 200 mg L⁻¹ (c); for the ZHN-MO sample for the initial concentration of 1000 mg L⁻¹. The ZHN-MO and ZHN phases are represented with * and ●, respectively.

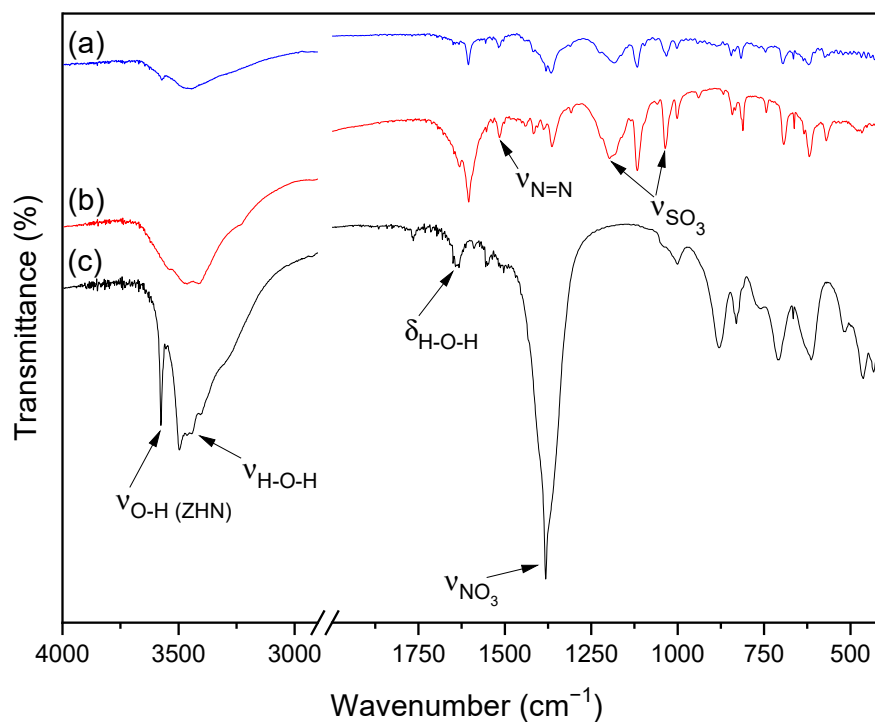


Figure 3. FTIR spectra of (a) MO, (b) the ZHN-MO sample for the initial concentration of 1000 mg L⁻¹ and (c) ZHN.

The FTIR spectra of MO (a) and ZHN-MO (b) present bands at 1207 and 1032 cm^{-1} , corresponding to sulfonate (SO_3), a characteristic of the methyl orange functional groups. In Figure 3, the band at 1383 cm^{-1} in spectrum (c) is characteristic of nitrate ions present on the surface and in the interlayer space of zinc hydroxide nitrate [25–27]. This band decreased in (b) due to the partial replacement of the NO_3 groups of ZHN by MO molecules, modifying its vibrational mode. The peak at 1520 cm^{-1} in (b), corresponding to the azo group ($\text{N}=\text{N}$), is the main evidence of the interaction of MO with ZHN, not presented in sample (c) of pure ZHN.

3.2. Adsorption Experiments

3.2.1. Effect of Initial MO Concentration

The amount of MO adsorbed at equilibrium and the removal percentage of the dye via adsorption onto ZHN at different temperatures and concentrations are shown in Table 1. More MO was adsorbed by the adsorbent as the initial dye concentration increased, but the removal percentage was lower. This behavior is due to the enhancement of MO's concentration gradient between the solution and the adsorbent surface, related to the increased initial concentration of adsorbate in the solution acting as a driving force in overcoming mass transfer resistance between the aqueous and the solid phases [28–31]. On the other hand, the percentage of MO removal was higher at lower dye concentrations. This result is related to the large number of occupied active sites compared with the amount of dye molecules present in the solution. In higher MO concentrations, the solutions promote the fast saturation of the adsorbent.

Table 1. Mass of MO adsorbed and percentage of removal at equilibrium by ZHN.

T (°C)	Initial Concentration of MO in mg L^{-1} (C_0)									
	100	200	300	400	500	600	700	800	900	1000
	Amount of MO Mass Adsorbed by ZHN in mg g^{-1} (q_e)									
25	49.9	97.2	148.0	197.3	243.1	280.4	288.4	361.5	413.2	413.2
45	49.1	99.0	148.8	198.0	247.9	296.4	336.0	357.4	405.2	431.6
55	48.3	96.0	144.8	185.8	240.3	240.3	299.1	301.9	316.1	346.4
	Percentage of Removal of MO by ZHN (%)									
25	99.4	99.4	99.8	99.5	98.5	97.5	98.9	94.3	91.2	91.3
45	97.8	99.0	99.1	99.5	99.4	99.3	98.6	97.2	96.7	90.8
55	96.9	96.0	96.1	94.5	96.1	92.8	91.9	75.5	72.6	71.2

The equilibrium uptake is an important part of the adsorption study to establish the capacity of an adsorbent to adsorb an adsorbate, taking into consideration the available active sites and the affinity between adsorbent dye in a dynamic balance.

The results obtained from the adsorption equilibrium are essential to calculate thermodynamic parameters, such as changes in enthalpy, entropy and Gibbs' free energy. These properties, in association with some others, will provide a mechanism for the adsorption of the system.

3.2.2. Effect of Contact Time

The adsorption equilibrium of the adsorbent for a particular adsorbate for different initial dye concentrations at the same temperature is usually dependent on the contact time and increases with the concentration, being an important parameter for the treatment of dye-containing wastewater [28,31]. In order to establish the optimum time for the maximum adsorption of MO onto ZHN, the adsorption process was carefully studied, following the time necessary to reach a constant level for each dye solution concentration and each temperature.

The contact time to achieve the adsorption equilibrium is shown in Figure 4. Hence, it is clear that the rate of MO uptake onto ZHN was more significant during the initial stages,

with the maximum equilibrium reached at 60 min for all the initial MO concentrations. The rapid adsorption of dye molecules is due to the large number of free active adsorption sites on the adsorbent and the relatively high concentration of dye molecules in the solution [29,32].

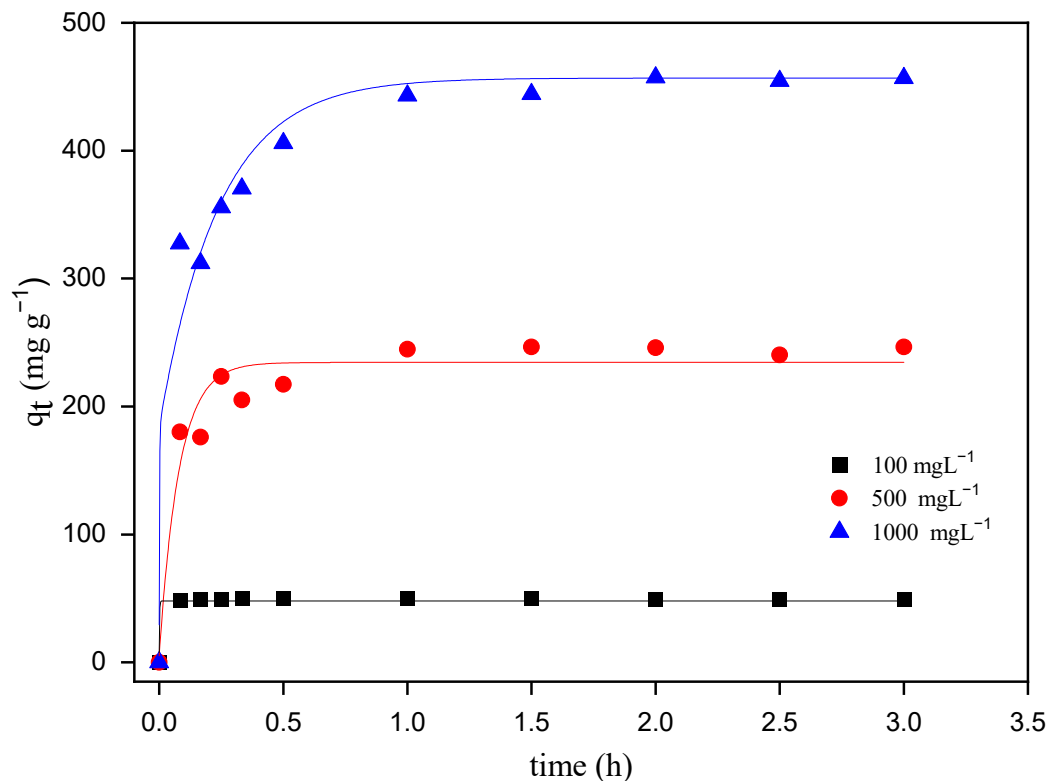


Figure 4. Effect of contact time on the adsorption of MO onto ZHN at three different initial MO concentrations at 25 °C.

3.2.3. Effect of Temperature

The temperature has a significant influence on the adsorption process of dyes, since it is directly related to the adsorption capacity of an adsorbent. In addition, increasing the temperature can reduce the viscosity of the solution, enabling the diffusion of the adsorbate molecules across the external boundary layer and in the internal pores of the adsorbent [26]. This study gives valuable information about the thermodynamic parameters, like enthalpy, entropy and Gibbs's free energy changes, associated with the adsorption process [31]. Figure 5 illustrates the effects of temperature on the adsorption of MO for the initial concentration of 400 mg L⁻¹.

The equilibrium adsorption capacity was clearly affected by the temperature (Figure 5). The adsorption of MO decreased from 197.3 mg g⁻¹ (99.5% removal) to 185.8 mg g⁻¹ (94.5% removal) when the temperature was raised from 25 to 55 °C. The decrease in MO removal for the highest temperature indicates not only that the temperature has a significant effect on adsorption, but also that the adsorption of MO onto the ZHN adsorbent surface is kinetically controlled via an exothermic process [29,32,33]. Therefore, the dominant mechanism expected is mainly physical, since, at the highest temperature, the desorption of dye molecules instead of adsorption occurs on the active sites of the adsorbent surface [29–31,34].

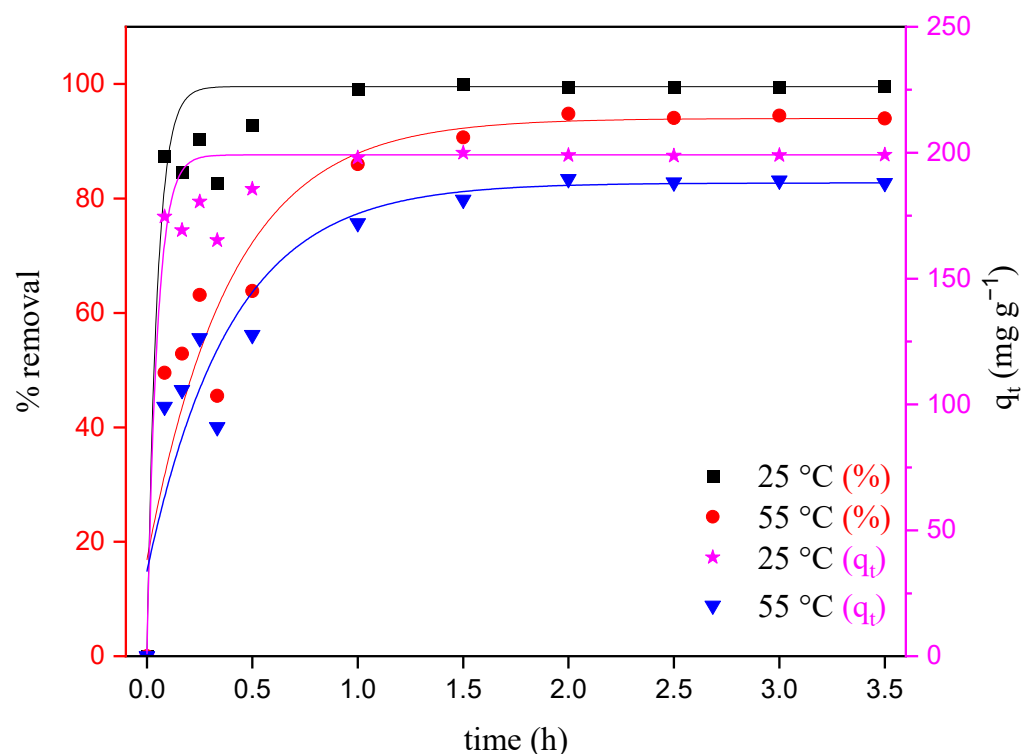


Figure 5. Effect of temperature on the adsorption of MO onto ZHN for a solution initially containing 400 mg L^{-1} of MO as a function of time.

3.2.4. Adsorption Isotherms

Adsorption isotherms are important for providing valuable insights related to the adsorption mechanism of a system. The adsorption isotherm describes the relationship between the adsorbate molecules adsorbed on the adsorbent surface and the adsorbate concentration remaining in the solution when the adsorption process reaches an equilibrium state. The data to fit the isotherm equations are the amount of adsorbate per mass unit of adsorbent (q_e) and the concentration of the adsorbate solution in equilibrium (C_e) at constant temperature [33,35]. The adsorption process was studied through the Langmuir and Freundlich adsorption models.

The linearized Langmuir form [36] is represented by Equation (2):

$$\frac{C_e}{q_e} = \frac{1}{QK_L} + \frac{C_e}{Q} \quad (2)$$

where q_e is the amount of MO adsorbed per weight unit of ZNH (mg g^{-1}); C_e is the equilibrium concentration of MO in the solution (mg L^{-1}); Q is the maximum adsorption capacity of the adsorbent for ZNH (mg g^{-1}); K_L is the Langmuir constant (L mg^{-1}).

The linearized Freundlich form [37] can be represented as follows (Equation (3)):

$$\ln q_e = \ln K_F + \frac{1}{n} \ln C_e \quad (3)$$

where K_F is the Freundlich constant (mg g^{-1}) ($\text{L}^{-1} \text{mg}^{-1}/n$) related to the adsorption capacity and n is an empirical parameter related to the adsorption intensity.

The applicability of the Langmuir or Freundlich models is generally assessed through evaluating the correlation coefficient (r). Table 2 shows a better fit of the experimental equilibrium adsorption data to the Langmuir ($r = 0.99548$) than to the Freundlich ($r = 0.57379$) model, which means that the process occurs via the adsorption of molecules to active sites on the adsorbent surface, forming a monolayer. The electrostatic interaction may play a major role in the adsorption between the negative charge of the dye and the positive resid-

ual charges of the adsorbent in order to neutralize the surface, instead of the substitution of nitrate groups in the interlamellar space by dye molecules as indicated by the X-ray results [35,37,38].

Table 2. Langmuir and Freundlich parameters.

T (°C)	Langmuir			Freundlich		
	K_L (L mg ⁻¹)	Q (mg g ⁻¹)	r	1/n	K_F (L g ⁻¹)	r
25	0.576	333.3	0.97063	0.297	101.955	0.80239
45	0.111	500.0	0.98597	0.348	90.357	0.66985
55	0.054	357.1	0.99548	0.384	52.558	0.57379

Abbreviations: K_L —constant of the theoretical adsorption capacity in the monolayer; Q—constant related to adsorption energy; K_F —Freundlich constant related to adsorption intensity; n —constant related to the adsorption intensity; r—linear correlation factor.

An important characteristic of a Langmuir isotherm can be expressed through a dimensionless constant separation factor, also called equilibrium parameter (R_L), which is related to the feasibility of the adsorption process [29,30,35] and can be expressed as (Equation (4)):

$$R_L = \frac{1}{1 + K_L C_0} \quad (4)$$

where C_0 is the adsorbate initial concentration (mg g⁻¹). The value of R_L indicates if the isotherm is unfavorable ($R_L > 1$), linear ($R_L = 1$), favorable ($0 < R_L < 1$) or irreversible ($R_L = 0$). The R_L values were found to be 0.00173, 0.000222 and 0.000151 at 25, 45 and 55 °C, respectively, indicating that the adsorption process is favorable.

3.2.5. Thermodynamic Parameters

Thermodynamic parameters are the properties of a system directly linked to the adsorption efficiency of an adsorbent, being related to the effect of the temperature [28–30,32]. Standard enthalpy ($\Delta_{ads}H^\circ$), standard entropy ($\Delta_{ads}S^\circ$) and standard Gibbs' free energy ($\Delta_{ads}G^\circ$) changes can be estimated using Equations (5) and (6):

$$\Delta_{ads}G^\circ = -RT \ln K_L \quad (5)$$

$$\ln K_L = -\frac{\Delta_{ads}H^\circ}{RT} + \frac{\Delta_{ads}S^\circ}{R} \quad (6)$$

where R is the gas constant ($R = 8.314 \text{ J mol}^{-1} \text{ K}^{-1}$); T the absolute temperature; K_L is the equilibrium Langmuir constant (L mg⁻¹). Equation (6) provides the enthalpy and entropy changes by plotting $\ln K_L$ versus T^{-1} (Figure 6).

The $\Delta_{ads}H^\circ$ e $\Delta_{ads}S^\circ$ values estimated from the slope and the intercept of the straight line passing through the points of the plot of $\ln K_L$ versus T^{-1} were $-63.77 \text{ kJ mol}^{-1}$ and -218.24 J K^{-1} , respectively. The $\Delta_{ads}G^\circ$ values were 1.27 kJ mol^{-1} , 5.63 kJ mol^{-1} and 7.81 kJ mol^{-1} at 25, 45 and 55 °C, respectively.

The negative values of $\Delta_{ads}H^\circ$ e $\Delta_{ads}S^\circ$ indicate an exothermic process and a decrease in the molecular organization of the adsorption process with a reduction in the randomness at the solid/liquid interface. Similar results have been found for different adsorbents and adsorbates [39–42].

The positive values of $\Delta_{ads}G^\circ$ at all temperatures indicate a non-spontaneous process. Since the $\Delta_{ads}S^\circ$ value is negative, this means that it has a strong influence on the $\Delta_{ads}G^\circ$ values (considering $\Delta_{ads}H^\circ$ is also negative).

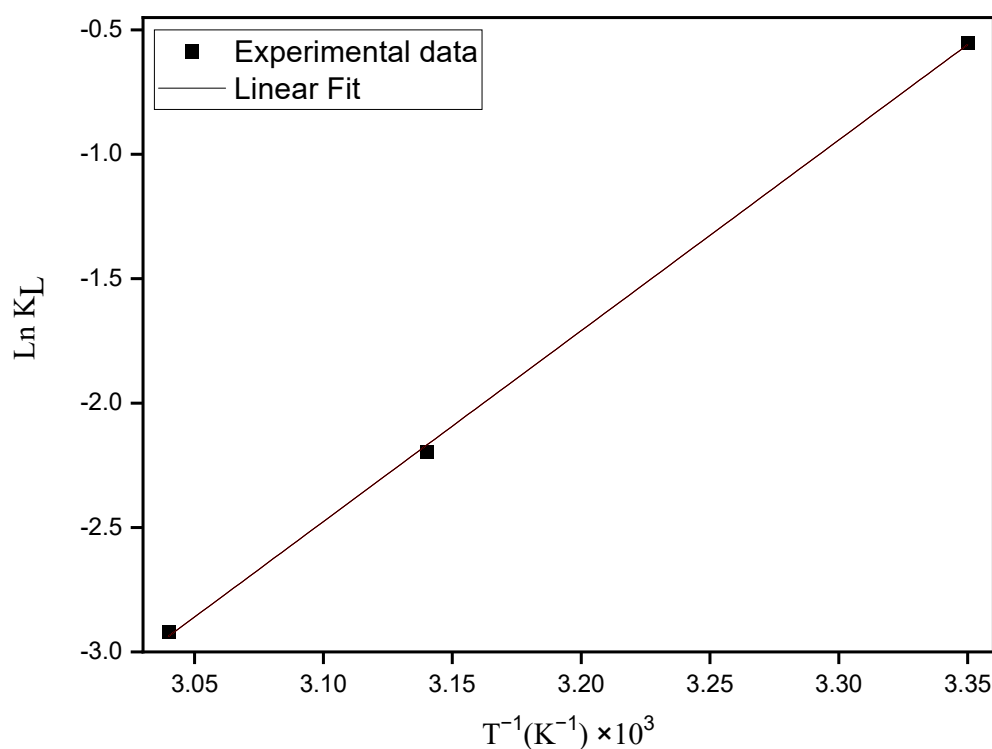


Figure 6. Van't Hoff plot for the adsorption of MO onto ZHN.

3.2.6. Kinetic Parameters

Valuable information about the adsorption pathways and the mechanism of the adsorption process can be obtained through studying kinetics, bringing many insights into treating aqueous effluents. The process involved in the adsorption of MO dye onto ZHN can be investigated using the pseudo-first- [43] and pseudo-second-order [44] kinetic models, Equations (7) and (8).

$$\ln(q_e - q_t) = \ln q_e - k_1 t \quad (7)$$

$$\frac{t}{q_t} = \frac{1}{k_s q_e^2} + \frac{t}{q_e} \quad (8)$$

where q_t and q_e are the mass of MO adsorbed (mg g^{-1}) at any time (h), and equilibrium k_1 and k_2 are the rate constants of a pseudo-first-order (h^{-1}) and pseudo-second-order ($\text{g mg}^{-1} \text{h}^{-1}$) kinetic process. The kinetic parameters k_1 and k_2 have been determined according to the plots of $\ln(q_e - q_t)$ versus t and t/q_t versus t (Equations (7) and (8), respectively). If applicable, the plots should give straight lines evaluated considering the highest correlation coefficient value (r_1 or r_2). All those parameters are shown in Table 3.

Table 3. Kinetic parameters of removal of MO from aqueous solution by ZHN at temperatures of 25, 45 and 55 °C.

T (°C)	Pseudo-First-Order				Pseudo-Second-Order		
	q_{exp} (mg g^{-1})	k_1 (min^{-1})	q_{calc} (mg g^{-1})	r_1	k_2 ($\text{g mg}^{-1} \text{min}^{-1}$)	q_{calc} (mg g^{-1})	r_2
25	413.21	-4.15	63.91	0.372	0.122	411.52	0.999
45	405.22	0.04	-0.453	0.790	0.040	429.18	0.999
55	316.11	0.15	-0.858	0.823	0.050	320.51	0.996

Table 3 shows the values obtained for the pseudo-first and pseudo-second-order kinetic parameters for the system at the three study temperatures. As shown in Table 3, r_2

was higher than r_1 at the three temperatures, and they were considering all the initial MO concentrations (not shown here), suggesting that the pseudo-second-order model may best describe the adsorption process [34].

The value of the activation energy was obtained using the temperature and rate constants obtained from the pseudo-second-order model through the Arrhenius equation, represented in Equation (9):

$$\ln k_{sm} = \ln A - \frac{E_a}{RT} \quad (9)$$

where k_{sm} is the rate constant obtained in the reaction process, A is the Arrhenius constant, E_a is the activation energy (kJ mol^{-1}), R is the universal gas constant ($8.314 \text{ J mol}^{-1} \text{ K}^{-1}$) and T is the absolute temperature (K).

The activation energy was obtained through the graph of $\ln k_{sm}$ versus T^{-1} (Figure 7) according to Equation (9). The value obtained was $105.45 \text{ kJ mol}^{-1}$, which characterizes a chemisorption process, since values between $5\text{--}40 \text{ kJ mol}^{-1}$ are characteristic of physical sorption, while values between $40\text{--}800 \text{ kJ mol}^{-1}$ refer to chemisorption [45,46].

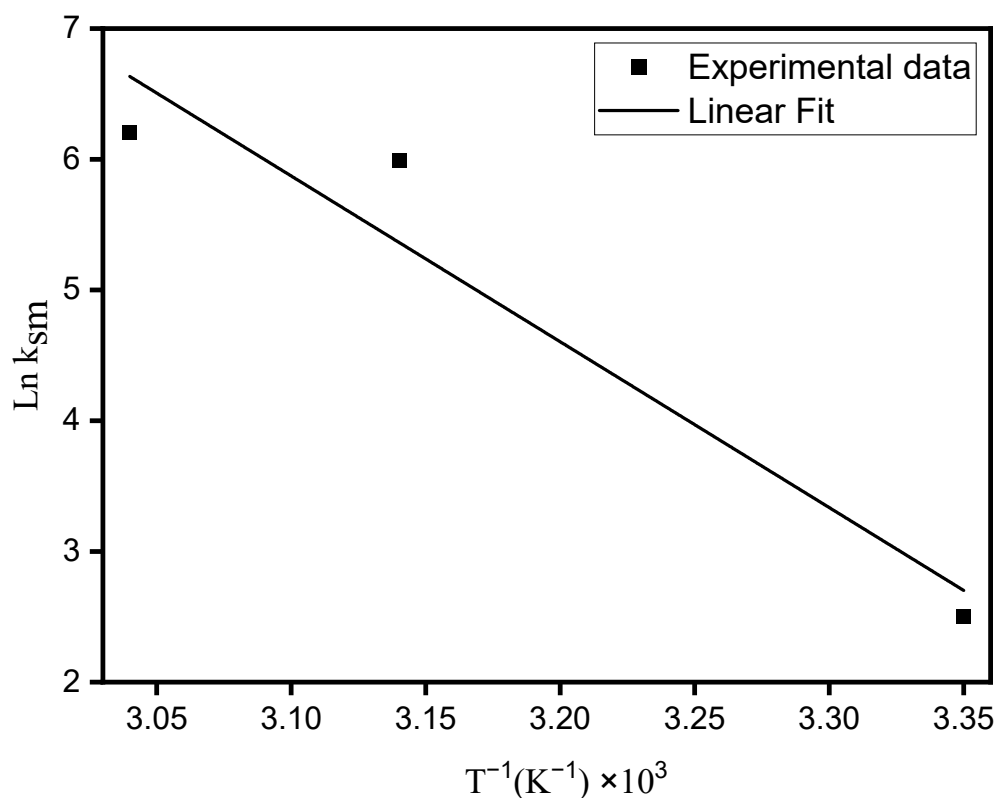


Figure 7. Arrhenius plot for MO adsorption from aqueous solution onto ZHN.

4. Conclusions

This study of the removal of methyl orange dye using zinc hydroxide nitrate proved to be efficient, with removals exceeding 90% in some cases. The thermodynamic study indicated an exothermic process, and the overall results were described using the Langmuir isotherm. The values of $\Delta_{\text{ads}}H^\circ = -65.32 \text{ kJ mol}^{-1}$ and $\Delta_{\text{ads}}S^\circ = -223.39 \text{ J K}^{-1} \text{ mol}^{-1}$ confirm the exothermic nature of the adsorption process and a decrease in randomness in the interface, while the value $\Delta_{\text{ads}}G^\circ$ indicates the non-spontaneous process. The overall rate of the sorption process appears to result from a pseudo-second-order mechanism with correlation coefficients higher than 0.96 for all initial concentrations and temperatures. According to the kinetic data, the activation energy was found to have a value of $105.45 \text{ kJ mol}^{-1}$; this value suggests the presence of the formation of chemical bonds between the adsorbate and adsorbent in the monolayer via the chemisorption process, concurrent with an intercalation process of the dye in the interlayer space of the ZHN, as

seen in the XRD patterns. Once, MO was a popular form of an anionic azo dye and was thus used as a model for azo dye adsorption research. As a result, it should be possible to remove other azo dyes using adsorptive methods involving zinc hydroxide nitrate. Finally, in the context of removing dyes from aqueous solutions through passivating them in the layered structure of the adsorbent, zinc hydroxide nitrate demonstrated characteristics that place it in a position with the potential to be an alternative material to be studied further in the treatment of effluents and waste containing azo anionic dyes.

Author Contributions: Conceptualization, D.A.d.R.N. and R.M.; methodology, D.A.d.R.N. and R.M.; formal analysis, D.A.d.R.N., C.A.P.A. and R.M.; investigation, D.A.d.R.N., T.M.P.Z. and M.V.M.; resources, C.A.P.A. and R.M.; writing—original draft preparation, D.A.d.R.N., C.A.P.A. and R.M.; writing—review and editing, D.A.d.R.N. and R.M.; visualization, D.A.d.R.N., C.A.P.A. and R.M.; supervision, R.M.; project administration, R.M.; funding acquisition, R.M. All authors have read and agreed to the published version of the manuscript.

Funding: This research was funded by CAPES [Finance Code 001] and CNPq [Grant Number 455906/2014-9].

Institutional Review Board Statement: Not applicable.

Informed Consent Statement: Not applicable.

Data Availability Statement: The data used to support the findings of this study are included within the article. Should further data or information be required, these are available from the corresponding author upon request.

Acknowledgments: The authors thanks the CCMN (UNICENTRO) for the analysis. D.A.R.N thanks CAPES for the scholarship.

Conflicts of Interest: The authors declare no conflict of interest.

References

1. Jemai, R.; Djebbi, M.A.; Boubakri, S.; Rhaiem, H.B.; Amara, A.B.H. Effective removal of methyl orange dyes using an adsorbent prepared from porous starch aerogel and organoclay. *Colorants* **2023**, *2*, 209–229. [[CrossRef](#)]
2. Brar, S.K.; Wangoo, N.; Sharma, R.K. Enhanced and selective adsorption of cationic dyes using novel biocompatible self-assembled peptide fibrils. *J. Environ. Manag.* **2020**, *255*, 109804. [[CrossRef](#)] [[PubMed](#)]
3. Vilar, J.C.J.; Cavalcanti, D.L.; Silva, C.A.A.; Andrade, R.F.S.; Takaki, G.M. Decolorization of black B azo dye by *Pseudomonas aeruginosa*. *Int. J. Microbiol. Appl. Sci.* **2015**, *4*, 720–728.
4. Meerbergen, K.; Willems, K.; Dewil, R.; Impe, J.V.; Appels, L.; Lievens, B. Isolation and screening of bacterial isolates from wastewater treatment plants to decolorize azo dyes. *J. Biosci. Bioeng.* **2018**, *125*, 448–456. [[CrossRef](#)]
5. Wu, Z.; Shan, X.; Li, Z. Preparation of a porous graphene oxide/alkali lignin aerogel composite and its adsorption properties for methylene blue. *Int. J. Biol. Macromol.* **2019**, *143*, 325–333. [[CrossRef](#)]
6. Shen, L.; Jiang, X.; Chen, Z.; Fu, D.; Li, Q.; Ouyang, T.; Wang, Y. Chemical reactive of novel amino acids intercalated layered double hydroxides in As(III) and As(V) adsorption. *Chemosphere* **2017**, *176*, 57–66. [[CrossRef](#)]
7. Yan, J.; Wang, W.; Wu, K.; Miao, L.; Huang, Y.; Yang, Y. Dehydrogenation of methylcyclohexane over Pt-Sn supported on Mg-Al mixed metal oxides derived from layered double hydroxides. *Int. J. Hydrogen Energy* **2018**, *43*, 9343–9352. [[CrossRef](#)]
8. Hou, X.-J.; Li, H.; He, P.; Sun, Z.; Li, S. Structural and electronic analysis of Li/Al layered double hydroxides and their adsorption for CO₂. *Appl. Surf. Sci.* **2017**, *416*, 411–423. [[CrossRef](#)]
9. Cordeiro, C.S.; Silva, F.R.; Wypych, F.; Ramos, L.P. Catalisadores heterogêneos para produção de monoésteres graxos (biodiesel). *Quim. Nova* **2011**, *34*, 477–486. [[CrossRef](#)]
10. Liao, C.; Liu, X.; Ren, Y.; Gong, D.; Zhang, Z. Catalytic deoxygenation of vanillin over layered double hydroxide supported Pd catalyst. *J. Ind. Eng. Chem.* **2018**, *68*, 380–386. [[CrossRef](#)]
11. Deng, X.; Huang, J.; Wan, H.; Chen, F.; Lin, Y.; Xu, X.; Ma, R.; Sasaki, T. Recent progress in functionalized layered double hydroxides and their application in efficient electrocatalytic water oxidation. *J. Energy Chem.* **2019**, *32*, 93–104. [[CrossRef](#)]
12. Arizaga, G.G.C.; Satyanarayana, K.G.; Wypych, F. Layered hydroxide salts: Synthesis, properties, and potential application. *Solid State Ion.* **2007**, *178*, 1143–1162. [[CrossRef](#)]
13. Takei, T.; Fuse, H.; Miura, A.; Kumara, N. Topotactic transformation of Ni-based layered double hydroxide film to layered metal oxide and hydroxide. *Appl. Clay Sci.* **2016**, *124–125*, 236–242. [[CrossRef](#)]
14. Wang, L.; Dou, Y.; Wang, J.; Han, J.; Liu, L.; Wei, M. Layer-by-layer assembly of layered double hydroxide/rubber multilayer films with excellent gas barrier property. *Compos. Part A Appl. Sci. Manuf.* **2017**, *102*, 314–321. [[CrossRef](#)]

15. Asiabi, H.; Yamini, Y.; Shamsayei, M. Highly selective and efficient removal of arsenic (V) chromium(VI) and selenium (VI) oxyanions by layered double hydroxide intercalated with zwitterionic glycine. *J. Hazard. Mater.* **2017**, *339*, 239–247. [[CrossRef](#)] [[PubMed](#)]
16. Yoneyama, S.; Kodama, T.; Fujii, Y.; Kikuch, H.; Fujita, W. Preparation, crystal structure, and magnetic properties of a copper hydroxy salt with diamond chain magnetic network. *CrystEngComm* **2014**, *16*, 10385–10388. [[CrossRef](#)]
17. Lee, A.-H.; Tanaka, M.; Takahashi, Y.; Kim, K.-W. Enhanced adsorption of arsenate and antimonate by calcined Mg/Al layered double hydroxide: Investigation of comparative adsorption mechanism by surface characterization. *Chemosphere* **2018**, *211*, 903–911. [[CrossRef](#)]
18. Eniola, J.O.; Kumar, R.; Al-Rashdi, A.A.; Barakat, M.A. Hydrothermal synthesis of structurally variable binary CuAl, MnAl and ternary CuMnAl hydroxides for oxytetracycline antibiotic adsorption. *J. Environ. Chem. Eng.* **2019**, *8*, 103535. [[CrossRef](#)]
19. Hidekazu, T.; Kaneda, R.; Fujioka, A.; Ishikawa, T. Synthesis of Ti (IV) substituted calcium hydroxyapatite microparticles by hydrolysis of phenyl phosphate. *J. Adv. Powder Technol.* **2010**, *21*, 169–170.
20. Gu, P.; Zhang, S.; Li, X.; Wang, X.; Wen, T.; Jehan, R.; Alsaedi, A.; Hayat, T.; Wang, X. Recent advances in layered double hydroxide-based nanomaterials for the removal of radionuclides from aqueous solution. *Environ. Pollut.* **2018**, *240*, 493–505. [[CrossRef](#)]
21. Haque, M.M.; Haque, M.A.; Mosharaf, M.K.; Marcus, P.K. Decolorization, degradation and detoxification of carcinogenic sulfonated azo dye methyl orange by newly developed biofilm consortia. *Saudi J. Biol. Sci.* **2021**, *28*, 793–804. [[CrossRef](#)] [[PubMed](#)]
22. Wu, L.; Liu, X.; Lv, G.; Zhu, R.; Tian, L.; Liu, M.; Li, W.; Rao, W.; Liu, T.; Liao, L. Study on the adsorption Properties of methyl Orange by natural one-dimensional nano-mineral materials with different structures. *Sci. Rep.* **2021**, *11*, 10640. [[CrossRef](#)] [[PubMed](#)]
23. Jaeger, S.; Nogueira, D.A.R.; Oliveira, D.S.; Machado, M.V.; Marangoni, R. Study of different morphology of zinc hydroxides salts as adsorbant of azo dyes. *ChemistrySelect* **2021**, *6*, 4354–4367. [[CrossRef](#)]
24. Hallajiqomi, M.; Hossein, E. Adsorption of manganese ion using polyaniline and its nanocomposite: Kinetics and isotherm studies. *J. Ind. Eng. Chem.* **2017**, *55*, 191–197. [[CrossRef](#)]
25. Oliveira, H.B.; Wypych, F. Comparative sorption studies of chromate by nano-and-micro sized Fe₂O₃ particles. *J. Solid State Chem. Sci.* **2016**, *243*, 136–145.
26. Louer, D.; Louer, M.J. Methode d'essais et erreurs pour l'indexation automatique des diagrammes de poudre. *J. Appl. Crystallogr.* **1972**, *5*, 271–275. [[CrossRef](#)]
27. Marangoni, R.; Ramos, L.P.; Wypych, F. New multifunctional materials obtained by the intercalation of anionic dyes into layered zinc hydroxide nitrate followed by dispersion into poly(vinyl alcohol)(PVA). *J. Colloid Interface Sci.* **2009**, *330*, 303–309. [[CrossRef](#)]
28. Almeida, C.A.P.; Debacher, N.A.; Downs, A.J.; Collet, L.; Mello, C.A.D.J. Removal of methylene blue from colored effluents by adsorption on montmorillonite clay. *J. Colloid Interface Sci.* **2009**, *332*, 46–53. [[CrossRef](#)] [[PubMed](#)]
29. Asif Tahir, M.; Bhati, H.N.; Lqbal, J.M. Solar Red brittle blue direct dye adsorption onto eucalyptus angophoroides bark: Equilibrium, kinetics and thermodynamic studies. *J. Environ. Chem. Eng.* **2016**, *4*, 2431–2439. [[CrossRef](#)]
30. Cui, M.; Johansson, K.H. Comparison of tungstate and tetrathiotungstate adsorption onto pyrite. *Chem. Geol.* **2017**, *464*, 57–68. [[CrossRef](#)]
31. Manzoor, Q.; Lqbal, M.; Saeed, R.; Ansari, T.M. Organic acids pretreatment effect on rosa brourbonia phyto-biomass for removal of Pb (II) and Cu(II) from aqueous media. *Bioresour. Technol.* **2013**, *132*, 446–452. [[CrossRef](#)] [[PubMed](#)]
32. Badawi, M.A.; Negm, N.A.; Kanac, M.T.H.; Hefnib, H.H.; Moneema, M.M.A. Adsorption of aluminum and lead from wastewater by chitosan-tannic acid modified biopolymers: Isotherms, kinetics, thermodynamics and process mechanics. *Int. J. Biol. Macromol.* **2017**, *99*, 465–476. [[CrossRef](#)] [[PubMed](#)]
33. Fernandes, A.N.; Almeida, C.P.A.; Menezes, C.T.B.; Debacher, N.A.; Sierra, M.M.D. Removal of methylene blue from aqueous solution by peat. *J. Hazard. Mater.* **2007**, *144*, 412–419. [[CrossRef](#)] [[PubMed](#)]
34. Almeida, C.A.P.; Santos, A.; Jaeger, S.; Debacher, N.A.; Hankins, N.P. Mineral waste from coal mining for removal of astrazon red dye from aqueous solution. *Desalination* **2010**, *264*, 181–187. [[CrossRef](#)]
35. Qiu, M.; Huang, C. Removal of dyes from aqueous solution by activated carbon from sewage sludge of the municipal wastewater treatment plant. *Water Treat.* **2015**, *53*, 3641–3648. [[CrossRef](#)]
36. Langmuir, I. The constitution and fundamental properties of solids and liquids. *Chem. Soc.* **1916**, *38*, 2221–2295. [[CrossRef](#)]
37. Freundlich, H.M.F.Z. Uber die adsorption in losungen. *Phys. Chem.* **1906**, *57*, 385–471.
38. Mahmound, M.E.; Nabil, G.M.; El-Mallah, N.M.; Bassiouny, H.I.; Kumar, S.; Abdel-Fattah, T.M. Kinetics, isotherms, and thermodynamics studies of the adsorption of reactive red 195 a dye from water by modified switchgrass biochass adsorbent. *J. Ind. Eng. Chem.* **2016**, *37*, 156–167. [[CrossRef](#)]
39. Ozer, A.; Akkaya, G.; Turabit, M. Biosorption of acid red 274(Ar274) on enteromorpha in a batch system. *J. Hazard. Mater.* **2005**, *126*, 119–127. [[CrossRef](#)]
40. Tay, C.C.; Redwan, G.; Liew, H.H.; Young, S.K.; Surif, S.; Adbuk, T.S. Copper(II) biosorption characteristic of Pleurotus spent mushroom compost. In Proceedings of the International Conference on Science and Social Research (CSSR), Kuala Lumpur, Malaysia, 5–7 December 2010; pp. 6–10.
41. Hawary, A.; Khraisheh, M.; Al-Ghouth, M.A. Characteristics of olive mill solid residue and its application in remediation of Pb₂₊, Cu₂₊ and Ni₂₊ from aqueous solution: Mechanistic studies. *Chem. Eng. J.* **2014**, *251*, 329–336. [[CrossRef](#)]

42. Bai, C.; Wang, L.; Zhu, Z. Adsorption of Cr(III) and Pb(II) by graphene oxide/alginate hydrogel membrane: Characterization, adsorption kinetics, isotherm and thermodynamics studies. *Int. J. Biol. Macromol.* **2020**, *147*, 898–910. [[CrossRef](#)]
43. Ho, Y.S. Citation review of langergrem kinetic rate equation on adsorption reaction. *Scientometrics* **2004**, *59*, 171–177.
44. Ho, Y.S.; Mckay, G. The kinetics of sorption of divalent metal ions onto sphagnum moss pear. *Water Res.* **2000**, *34*, 735–742. [[CrossRef](#)]
45. Zhao, J.; Huang, Q.; Liu, M.; Dai, Y.; Chen, J.; Huang, H.; Wen, Y.; Zhu, X.; Zhang, X.; Wei, Y. Synthesis of functionalized MgAl-Layered double hydroxides via modified mussel inspired chemistry and their application in organic dye adsorption. *J. Colloid Interface Sci.* **2017**, *505*, 168–177. [[CrossRef](#)] [[PubMed](#)]
46. Santos, S.C.R.; Boaventura, R.A.R. Adsorption of cationic and anionic azo dyes on sepiolite clay: Equilibrium and kinetic studies in batch mode. *J. Environ. Chem. Eng.* **2016**, *4*, 1473–1483. [[CrossRef](#)]

Disclaimer/Publisher's Note: The statements, opinions and data contained in all publications are solely those of the individual author(s) and contributor(s) and not of MDPI and/or the editor(s). MDPI and/or the editor(s) disclaim responsibility for any injury to people or property resulting from any ideas, methods, instructions or products referred to in the content.